CHAPTER IV
RESULTS AND DISCUSSION

4.1 Rise Velocity of a Single Bubble

The dependence of rise velocity of single bubbles moving in the fluidized bed on the bubble diameter is shown in Figure 4.1. The rise velocities increased rapidly for small diameters and increased slowly for large diameters. To obtain the equation for predicting the rise velocity of the single bubble in the fluidized bed, the results of the rise velocities at different bubble sizes were related to the rise velocity from the Equation 2.8. The rise velocity from the experiment was:

$$U_b = 0.447 (g D_e)^{1/2} \qquad (4.1)$$

and depended on the bubble diameter. Due to the wall effect the experimental rise velocity was slower than one in a fluid of infinite extent. The deviation of the experimental rise velocity compared to the rise velocity by Maneri and Mendelson (1968) or Equation 2.8 was lower than 20.77% as shown in Figure 4.2. There were two reasons for the deviations. First, the rise velocity depended on the type of particles. This reason was confirmed by the experiments using seeds (Green Kuang Futsoi, diameter 1.5 mm, density 1.063 g/cm^3, void fraction 0.4803, incipient fluidized velocity 66.67 cm/s) for which the rise velocity was $U_b = 0.312 (gD_e)^{1/2}$. The rise velocity of the single bubble using the large particles was less than one using the small particles because the wake or the retarding force opposing the motion of bubble behind the bubble was high with the large particles (Harrison and Davidson, 1971). Second, single bubbles initially growing in a spherical shape were subsequently compressed into cylindrical shapes by the parallel plates, so the front sides and

back sides of the bubbles contacted the wall during the bubble movement and resisted the bubble movement.

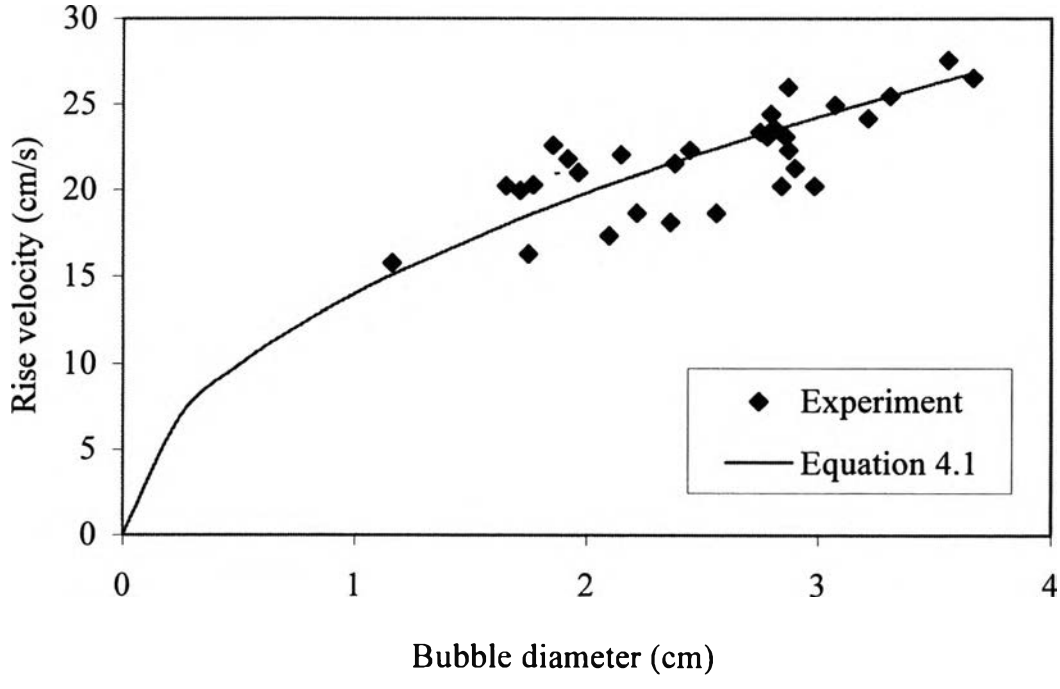

Figure 4.1 Rise velocity of single bubbles in two-dimensional fluidized bed containing stone particles 0.212-0.250 mm in diameter.

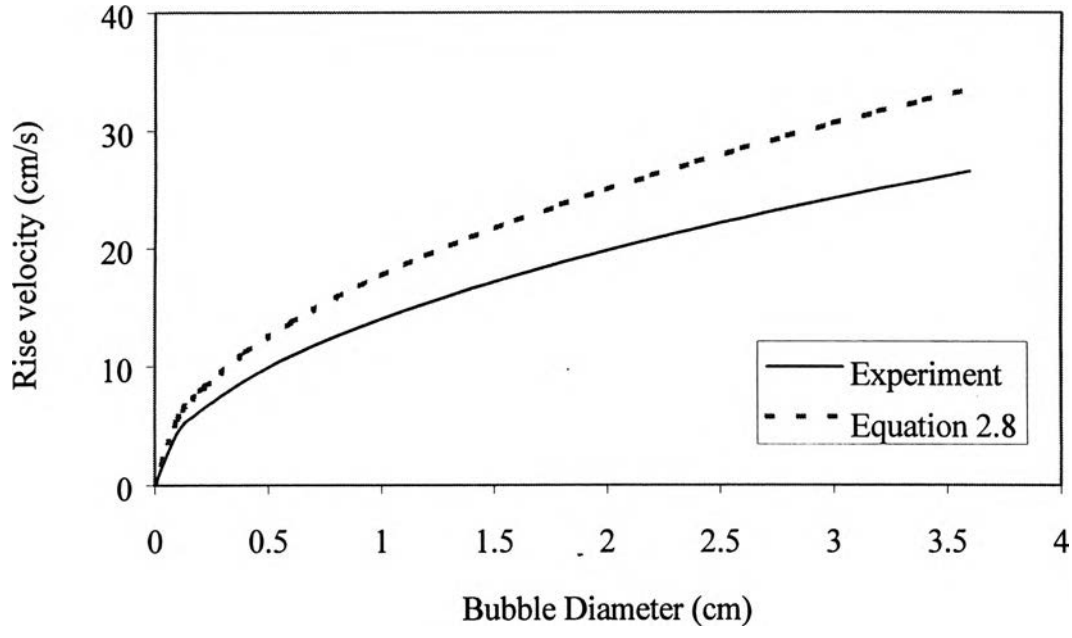

Figure 4.2 Comparison of experimental rise velocity of single bubbles with those predicted for an infinite fluid by Equation 2.8.

4.2 The Volume of the Bubble Formed at an Orifice

By flowing air through the orifice, the bubble grew until its radius equaled the orifice-to-bubble-center-distance and detached from the orifice. The air flow rates generating the bubble at the orifice affected the size of the bubbles as shown in Figure 4.3. At low flow rates small bubbles developed easily and many bubbles were present in the bed. At the high flow rates, the time for generating the bubbles was higher than one at the low flow rates, and the bubble size was larger and there was a smaller number of bubbles presented in the bed.

The relation between the bubble volume and the air flow rate from the experiment was:

$$V_b = 0.318 G^{4/3} / g^{2/3} \qquad (4.2)$$

The deviation of the bubble volume between Equation 4.2 and Equation 2.2 or $V_b = 2.168\ G^{4/3}/g^{2/3}$ was lower than 85.33%.

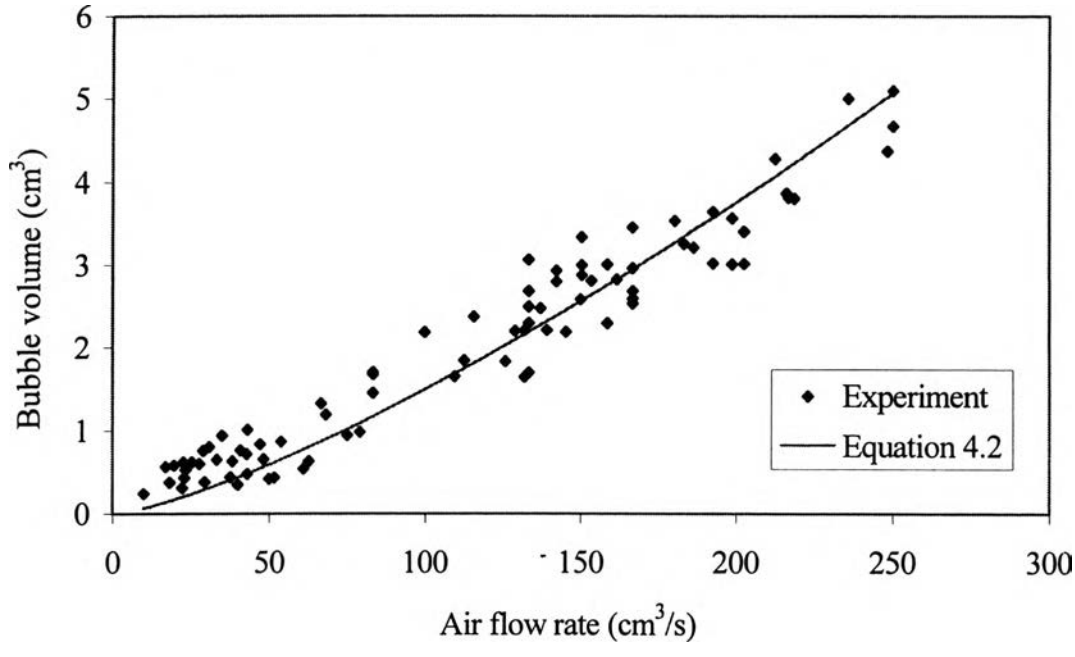

Figure 4.3 Volume of bubbles detached from the orifice in the fluidized bed containing stone particles 0.212-0.250 mm in diameter.

This relation denoted that the bubble volume depended on the air flow rate. The large deviations were caused by three factors. First factor was the circulation of air between the bubble and the particulate phase. During the bubble growth, the air leaked through the bubble roof into the particulate phase, whereas particulate phase air entered the bubble at the bubble base. Because of the inequality between the leakage air and the entering air, the bubble volume in the experiment was distorted from the ideal case. Second factor was the acceleration of the solids around the bubble. The solids around the lower surface of the bubble accelerate faster than the solids at the upper surface. As a result, the bubble detached before the radius of the bubble was the same as the orifice-to-bubble-center-distance. Third factor was a wake formed below the bubble. After the bubble separated from the orifice, the

wake carried the solids into the bubble. The wake caused the circulating current near the orifice to disturb the formation of the bubble.

To consider the air leakage from the bubble, the air mass balance (Equation 2.9) and the momentum balance (Equation 2.10) were applied to determine the bubble sizes at the different superficial air leakage velocities from the bubble (the superficial air leakage velocity was the volumetric flow rate of leakage air from the bubble per surface area of the bubble or $\pi D_e T$) as shown in Figure 4.4.

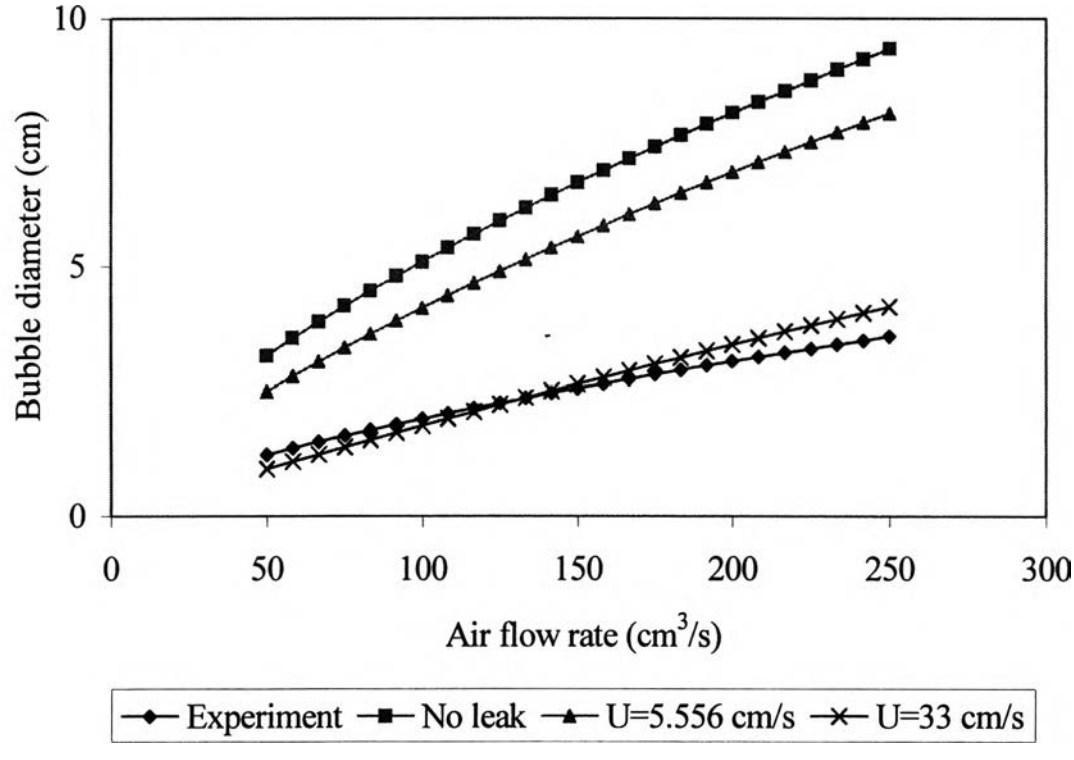

Figure 4.4 Variation of the bubble diameters detached from the orifice with the air flow rates at different gas leakage velocities.

The superficial air leakage velocity was obtained by simultaneous numerical integration of Equations 2.9 and 2.10, and the condition of the bubble detachment was imposed at $s = r_b$. By estimating the superficial air leakage velocity in the experiment, the experimental diameters from Equation

4.2 and the theoretical results of the bubble diameters from Equation 2.9 and 2.10 were related at the different superficial air leakage velocities until the curve of theoretical results between the bubble diameters and the air flow rate approached the curve of experimental results. The corresponding superficial air velocity in the experiment was 33 cm/s. At low superficial air leakage velocities or no leakage at all, the bubble sizes were higher than those at high velocities. From the two-phase theory of fluidization, the superficial air velocity in the particulate phase equaled to the air incipient fluidizing velocity but the superficial air leakage velocity from the bubble surface to the particulate phase was above the incipient fluidizing velocity. Deviation from this theory was possible since the void fraction was not constant and gas channeling occurred in the bed. Since the superficial air leakage velocity from the calculation was the velocity at the surface of the bubble but not the superficial air leakage velocity in the particulate phase.

The time required for the bubble detachment or the time required for generating the bubble was approximated from Equations 2.8 and 2.9 at $s = r_b$ when the superficial air leakage velocity was 33 cm/s, as shown in Figure 4.5. The detachment time was a function of the air flow rate. The small bubbles were generated easily and the frequency of the bubble formation was high at the low air flow rate. Concerning the effect of the superficial air leakage velocity on the detachment time of the bubbles, the detachment time at the high superficial air leakage velocity was less than the time for no air leakage. Because of the air leakage during the formation, the rate of accumulation of bubble mass was shorter and hence took less time for detachment.

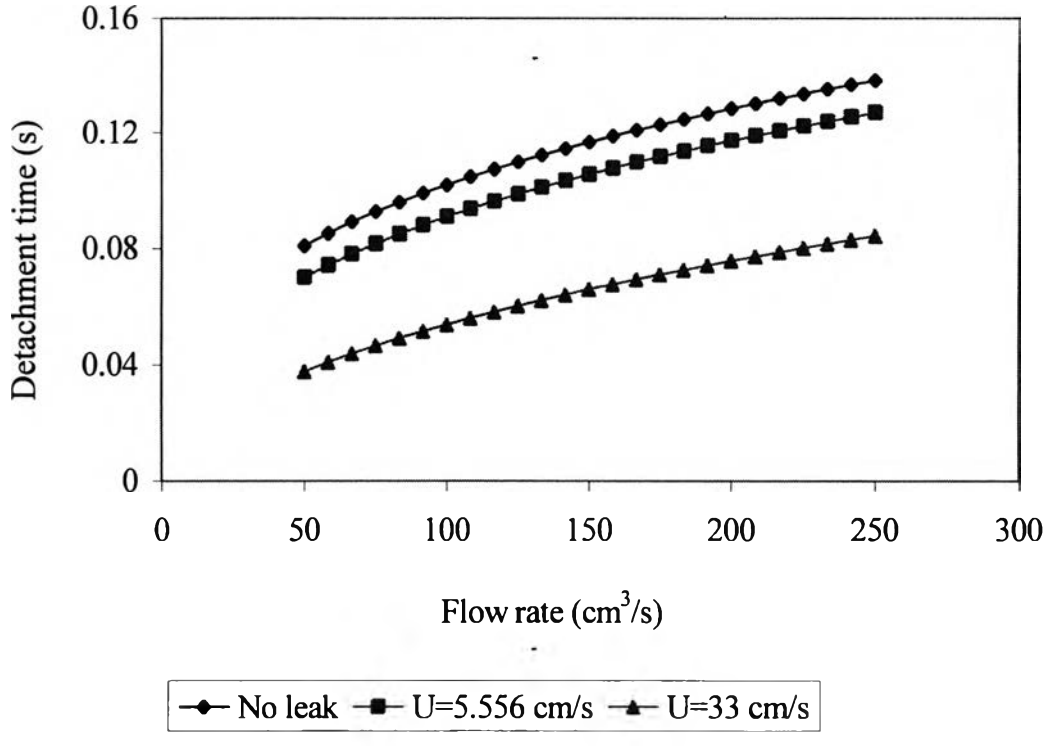

Figure 4.5 Comparison of the detachment times with the air flow rates at different gas leakage velocities.

To recognize the leakage of air into the particulate phase during the process of bubble formation by injecting air through an orifice in the fluidized state. The relation between observed bubble volumes with inlet volumetric air flow rates and frequencies of the bubble formation from that the superficial air leakage velocity of 33 cm/s was shown below:

$$V_b = 0.1586\left(\frac{Q_{or}}{n_b}\right)^{1.24} \qquad (4.3)$$

From Figure 4.6 the characteristic of this equation was parabolic that the amount of air leakage from the bubble was varied with the air flow rates and declined with increasing air flow rate or decreasing the frequency. This

equation was different from Equation 2.13 that the amount of air leakage from the bubble was constant.

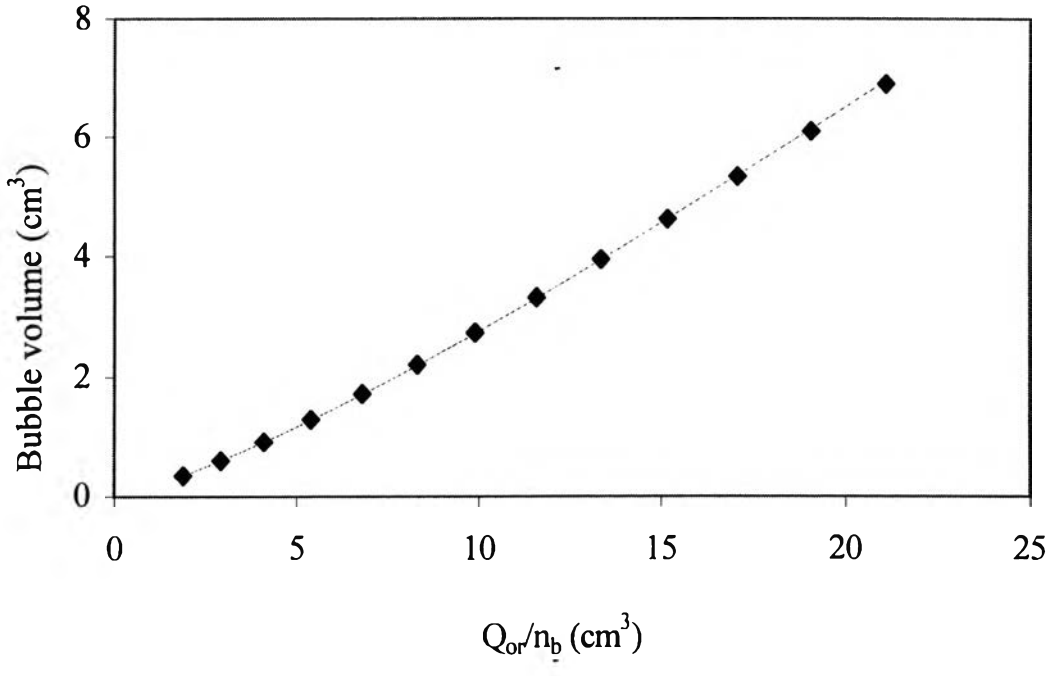

Figure 4.6 Relation of bubble volumes with different volumetric air flow rates and frequencies of the bubble formation.

The percentage of leakage air from the top of the bubble detaching from the orifice to the particulate phase is shown in Figure 4.7. The percentage of air leakage from Equation 2.12 declined when the bubble diameter increased. Because of the air exchange between the bubble phase and the particulate phase, the large bubble that had a high detachment time obtained the air entering the bubble at the base from the particulate phase to overcome the leakage air leaving the bubble at the roof.

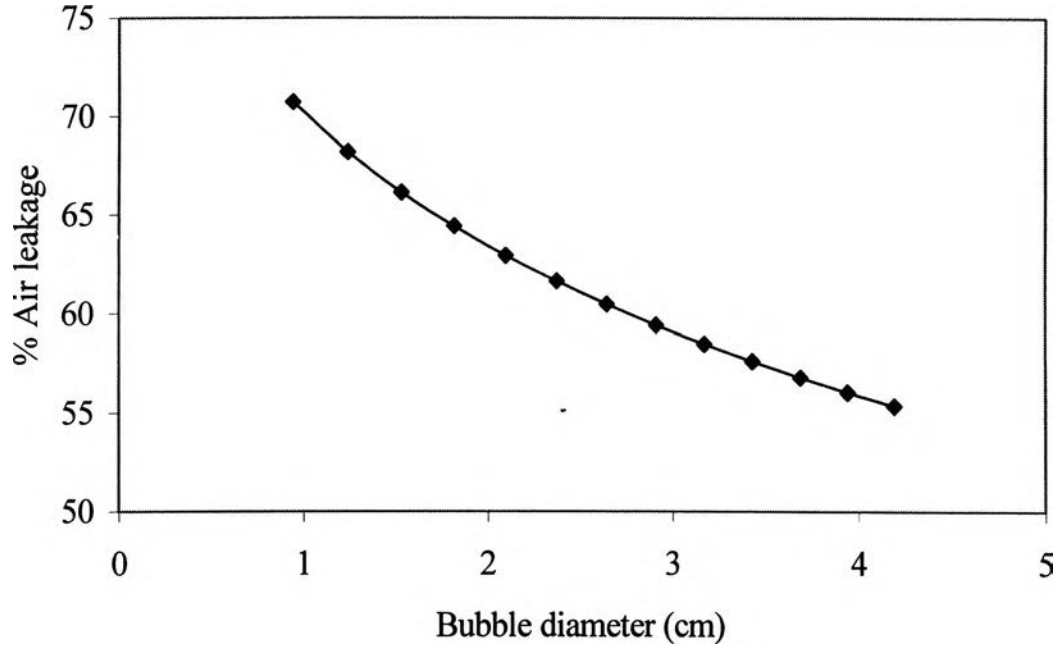

Figure 4.7 Percentage of air leakage from the bubble detaching from the orifice at different bubble diameters.

4.3 The Rise Velocity of a Continuous Swarm of Small Bubbles

During the generation of the bubbles in the fluidized bed by increasing the air flow rate above that required for incipient fluidization, the bed expanded as shown in Figure 4.8. This expansion occurred because the bubbles were present in the bed to increase its total volume.

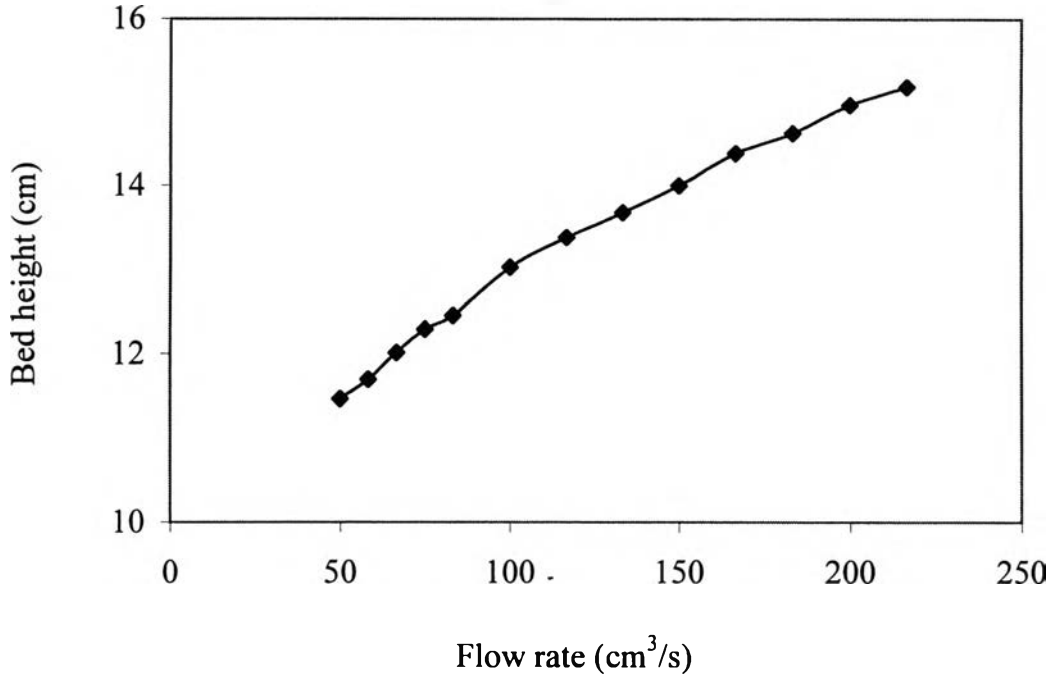

Figure 4.8 Height of the fluidized bed above incipient fluidization at the different air flow rates.

Although the rise velocity of each individual bubble depended on the bubble size, the rise velocity of the bubble in the expanded bed was higher than one in the incipiently fluidized bed. To predict the rise velocity in the expanded bed by increasing air flow rates and the bed heights at the incipient fluidization by assuming the uniform air flow rate above the incipient fluidization passing through the bed as the bubbles. From this assumption, the rise velocity of single bubbles at the incipiently fluidized bed were obtained from Equation 2.5 and the diameter of the bubbles in bed were obtained from Equation 4.1 are shown in Figure 4.9. The rise velocity and the bubble diameter increased with increasing air flow rate. Increasing the air flow rate also increased pressure in the bed as the pressure in the upper bed surface was constant or equaled to atmospheric pressure. At high air flow rates the pressure drop between the upper surface of the bed and the distributor

increased; this effect was the driving force for increasing the rise velocity of the bubble since the bubbles enlarged as the pressure drop increased.

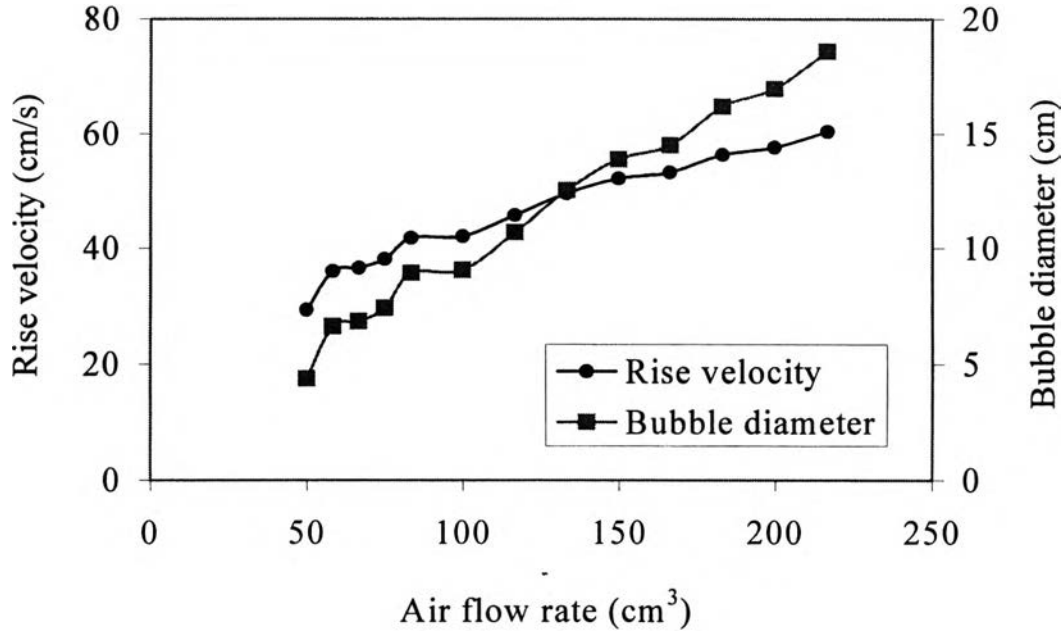

Figure 4.9 Variation of the rise velocities and the bubble diameters with the different air flow rates.

The bubble diameters and the rise velocities, shown in Figure 4.9, were obtained from the bubbles generated from the small holes on the gauze or porous distributor. The bubbles from the porous distributor were generated at all locations on the distributor, so the air distribution was uniform throughout the cross sectional area of the bed. In these phenomena the excess air flow rate above incipient fluidization formed the bubbles and there was no air channeling in the bed. The bubble diameters and the rise velocities were not the same as the bubbles generated from the perforated distributor from the experiment. The air distribution from the perforated distributor (28 holes) was only uniform near the holes that air flowed into the bed and the experimental bubbles were only generated at the holes. The number of bubbles and sizes depended on the number of holes on the distributor and the air flow rate. In

the experiments the bubbles coalesced and the sizes of bubbles varied with the vertical position in the bed, whereas the computed bubbles were based on no coalescence and constant size of the bubbles.

To consider the bubbles at different air flow rates, the volumetric bubble flow rate of the total bubbles at the surface of the distributor was related empirically to the bed height and the excess air flow rate above that needed for incipient fluidization, giving:

$$\frac{Q_b}{A} = 0.0417\,(U - U_{mf})^{0.0178}\, h^{2.606} \qquad (4.4)$$

The volumetric bubble flow rate of the total bubbles was the number of holes multiplied by bubble volume generated from the distributor per time. The volume of the bubble at the different flow rates from Equation 4.2 was used to estimate the diameter of bubble. The rise velocity of the bubble was computed from Equation 4.1 and the volumetric bubble flow rate of the single bubble was the product of the rise velocity multiplied by the perimeter of the bubble $(p = 2D_b + 2T)$. Increasing air flow rate resulted in the higher volumetric air flow rate as appeared as bubbles and the bed expansion. Bubbles continued to grow and to coalesce while they rose through the bed.

4.4 Movement of Air in the Fluidized Bed

To study the motion of the air, a single bubble was held or drawn within a rectangular region of the fluidized bed and the FORTRAN source code was used for displaying the air streamlines in the fluidized bed. By dividing the region into the elements and creating the equation of each element corresponding to the partial differential equation. The air streamlines were affected by the magnitude of the incipient interstitial fluidizing velocity u_i,

($u_i=U_{mf}/\varepsilon$), as compared to the rise velocity of the single bubble U_b. The incipient superficial air velocity in the fluidized bed U_{mf} was 5.127 cm/s and the void fraction was 0.4803, so the incipient interstitial fluidizing velocity was 10.675 cm/s. Since the rise velocities of the single bubble in the fluidized bed depended on the bubble diameters, the air streamlines were also affected by the bubble diameters.

4.4.1 $U_b < u_i$ for the Case in Which the Bubble Diameter < 0.6 cm

Because the rise velocity of the single bubble was less than the incipient interstitial air velocity, the upward flow of air entered at the lower half of the bubble and left at the upper half of the bubble as shown in Figure 4.10. The air streamlines penetrated into the bubble at the lower half since the permeability of the bubble was higher than that of the particulate phase, and the pressure in the lower part of the bubble was less than in the surroundings at the same level of the fluidized bed. To improve the efficiency of the interchange of air between the bubble and the remote parts of fluidized bed, the rise velocity or the bubble diameter was reduced.

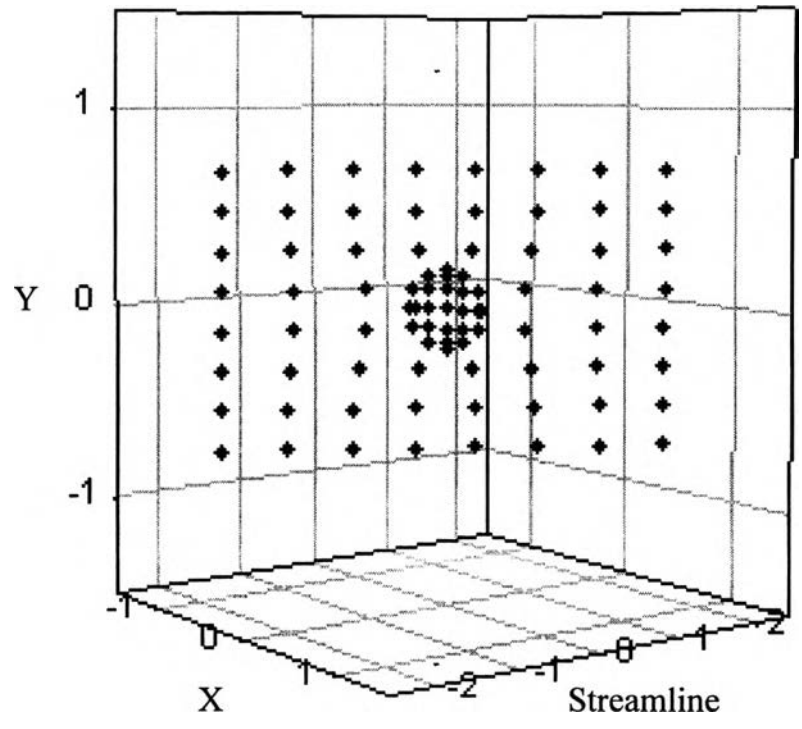

Figure 4.10 The streamlines of air in the single bubble when the rise velocity U_b was less than the incipient interstitial air velocity u_i.

4.42 $U_b > u_i$ for the Case in Which the Bubble Diameter > 0.6 cm.

In this case, the rise velocity of the single bubble was higher than the incipient interstitial air velocity. The air streamlines were completely different from the streamlines for the previous case. Air entering and leaving the bubble was confined to a small zone around the bubble. The limit of penetration represented a cylindrical disc of radius, R, compared to the bubble radius, r_b, which was calculated from the following equation relating U_b and u_i.

$$\frac{R^2}{r_b^2} = \frac{U_b + u_i}{U_b - u_i} \qquad (4.5)$$

The cylindrical disc as shown in Figure 4.11 was the limit of penetration of air. The size of the cylindrical disc was larger than the bubble

size, as shown in Figure 4.10. Outside the cylindrical disc, the fluidizing air flowed downward direction around it. Inside the bubble, there was the air circulation around the bubble, air flowed out at the upper part of the bubble and flowed in at the low part. The reason was the pressure gradient in the bubble. The air streamlines flowed out at the top of the bubble due to the high pressure gradient and they re-entered at the bottom of the bubble due to the low pressure gradient. Since the limit of penetration depended on U_b and u_i, the radius of penetration at the high air flow rate R approached the radius of the bubble, and air interchange between the bubble contacted with the particles only in a small zone in the vicinity of the bubble.

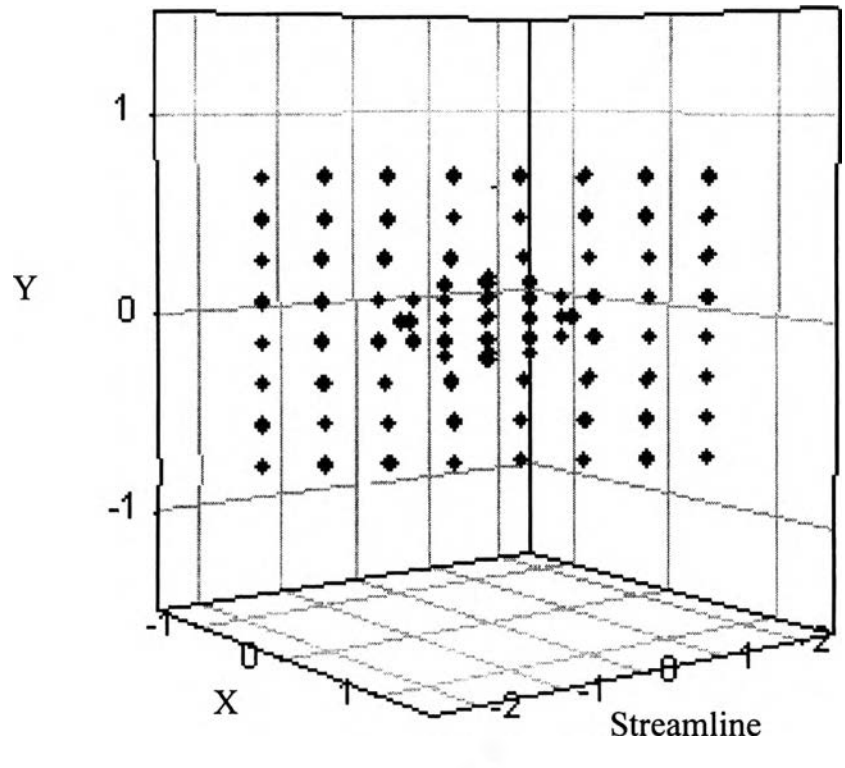

Figure 4.11 The stream lines of air in the single bubble when the rise velocity U_b was greater than the incipient interstitial air velocity u_i.